# Resolving Discrepancies in Spin-Torque Ferromagnetic Resonance **Measurements: Lineshape versus Linewidth Analyses**

Saba Karimeddiny<sup>1,\*</sup> and Daniel C. Ralph<sup>1,2</sup> <sup>1</sup>Cornell University, Ithaca, New York 14850, USA <sup>2</sup>Kavli Institute at Cornell, Ithaca, New York 14853, USA

(Received 6 March 2021; accepted 21 May 2021; published 7 June 2021)

When spin-orbit torques are measured using spin-torque ferromagnetic resonance, two alternative ways of analyzing the results to extract the torque efficiencies—lineshape analysis and analysis of the change in linewidth versus direct current—often give inconsistent results. We identify a source for these inconsistencies. We show that fits of spin-torque ferromagnetic resonance data to the standard analysis framework leave significant residuals that we identify as due to (i) current-induced excitations of a small volume of magnetic material with magnetic damping much larger than that of the bulk of the magnetic layer, which we speculate is associated with the heavy-metal-magnet interface and (ii) oscillations of the sample magnetization at the modulation frequency due to heating. The dependence of the residual signals on direct current can interfere with an accurate extraction of spin-torque efficiencies by the linewidth method. We show that the discrepancies between the two types of analysis can be largely eliminated by extrapolation of the window of magnetic fields used in the linewidth fits to small values so as to minimize the influence of the residual signals.

DOI: 10.1103/PhysRevApplied.15.064017

#### I. INTRODUCTION

Magnetic manipulation by spin-orbit torques (SOTs) [1,2] is a promising candidate mechanism for nextgeneration magnetic memory technologies [3,4]. Accurate, consistent measurements of the efficiencies of SOTs are essential for fully understanding the microscopic origin of SOTs and for the development of SOT memory technologies; yet despite the large body of work amassed on SOTs, quantitative discrepancies between different measurement techniques persist. Here we focus on inconsistencies that result from two approaches for analyzing spin-torque ferromagnetic resonance (ST FMR) measurements, the mostcommon experimental method used to quantify SOTs in heterostructures that have in-plane magnetic anisotropy [2,5–7]. These two approaches are lineshape (LS) analysis, in which the in-plane and out-of-plane spin-orbit torques are determined from the amplitudes of the symmetric and antisymmetric resonance components [2,5,8], and linewidth (LW) analysis, in which the dampinglike inplane component is determined from the dependence of the resonant linewidth on direct current (dc) [5,9-11]. These approaches often give results for the dampinglike spinorbit torque that differ by large factors (e.g., in the data we present below a difference by more than a factor of 3).

Here we investigate the cause of the discrepancy by performing ST-FMR measurements on Pt/permalloy (Py) and Pt/Co<sub>40</sub>Fe<sub>40</sub>B<sub>20</sub> samples, comparing data acquired using amplitude modulation of the microwave current (the mostcommon approach) and using frequency modulation, and by analyzing carefully the residuals in fits to the standard ST-FMR analysis for both modulation schemes. We identify that the discrepancies between the lineshape and linewidth analyses arise primarily from current-induced excitation of a small volume of magnetic material with magnetic damping much greater than that of the majority of the magnetic film. This produces a low-amplitude background ST FMR with a broad tail, which can interfere with accurate determination of dc-induced changes in the linewidth of the primary resonance. We demonstrate that discrepancies between the lineshape and linewidth analyses can be reduced by use of frequency modulation rather than amplitude modulation of the microwave current, and by extrapolation of the range of the magnetic field used in the linewidth fits to small values so as to minimize the disruption from the low-amplitude, large-linewidth artifact signal.

# II. BACKGROUND ON THE ST-FMR TECHNIQUE

During ST FMR, a microwave current is applied in plane into a heavy-metal-ferromagnet bilayer so that current-induced SOTs and Ørsted fields induce ferromagnetic precession. Magnetic precession causes

<sup>\*</sup>sabakarimeddiny@gmail.com

resistance variations in the device due to anisotropic magnetoresistance. Mixing between the microwave current and resistance oscillations then produces a dc voltage, which is measured. The signal-to-noise ratio is vastly increased if an endogenous parameter of the technique is modulated and the voltage is measured with a lock-in amplifier. There are a number of choices for the modulated parameter: amplitude modulation (AM) [2,5], magnetic field modulation [12], frequency modulation (FM), or phase modulation (the last two of which are equivalent). Save a few studies that have used magnetic field modulation [12–17], almost all experiments featuring ST FMR use AM because it is the simplest parameter to modulate—it does not complicate the experimental apparatus or the fitted model.

Typically, one assumes that a macrospin approximation is appropriate for describing the current-induced magnetic dynamics for experiments performed at sufficiently large microwave frequencies and magnetic fields, in which case the results of ST FMR are modeled by the Landau-Lifshitz-Gilbert-Slonczewski equation:

$$\dot{\mathbf{m}} = -\gamma \,\mathbf{m} \times \mathbf{B} + \alpha \,\mathbf{m} \times \dot{\mathbf{m}} + \boldsymbol{\tau},\tag{1}$$

where **m** is the magnetic moment,  $\gamma = 2\mu_B/\hbar$  is the gyromagnetic ratio, **B** is the external field,  $\alpha$  is the Gilbert damping constant, and  $\tau = \tau_{DL} + \tau_z$  describes the torque present in our system. The torques produced by a polycrystalline thin film must obey Rashba symmetry [18]. For a film spanning the X-Y plane with current flowing along the X direction we have

$$\tau_{\rm DL} = \tau_{\rm DL}^0[\mathbf{m} \times (\mathbf{m} \times Y)] = \frac{\xi_{\rm DL} \mu_B}{e M_s t_F} J_e \cos \phi_0, \quad (2)$$

$$\tau_z = \tau_z^0(\mathbf{m} \times Y)$$

$$= \left(\frac{\xi_{\text{FL}}\mu_B}{eM_s t_F} + \frac{\mu_0 t_N}{2}\right) J_e \cos \phi_0, \qquad (3)$$

where  $\xi_{\mathrm{DL(FL)}}$  is the dampinglike (fieldlike) SOT efficiency,  $\mu_B$  is the Bohr magneton,  $M_s$  is the saturation magnetization of the ferromagnet,  $t_F$  ( $t_N$ ) is the thickness of the ferromagnet (normal-metal) layer,  $\mu_0$  is the vacuum permeability,  $J_e$  is the electric current density flowing through the heavy metal, and  $\phi_0$  is the angle between the direction of the applied field and current flow (X direction). Solutions to the Landau-Lifshitz-Gilbert-Slonczewski equation for a sample with in-plane magnetic anisotropy predict that resonant ferromagnetic precession will occur when the Kittel equation,  $\omega_0 = \gamma \sqrt{B(B + \mu_0 M_{\mathrm{eff}})}$  [19], is satisfied. Here  $\mu_0 M_{\mathrm{eff}} = \mu_0 M_s - 2K_{\perp}/M_s$  accounts for shape anisotropy minus any out-of-plane anisotropy. The total resonance lineshape will have contributions from symmetric (S) and antisymmetric (S) Lorentzians [5,7], which we

define as

$$S = \frac{\Delta^2}{(R - R_0)^2 + \Delta^2},\tag{4}$$

$$A = \frac{\Delta(B - B_0)}{(B - B_0)^2 + \Delta^2},\tag{5}$$

where  $B_0$  is the resonance field and  $\Delta$  is the half-width-at-half-maximum linewidth related to the Gilbert damping by  $\Delta = \alpha \omega / \gamma$ . The dc mixing signal is a weighted sum of these two lineshapes with coefficients  $V_S$  and  $V_A$  determined by the torques and the material parameters in our system [5,7,20]:

$$V_{\text{mix}} = V_S S + V_A A + C, \tag{6}$$

with

$$V_{S} = \frac{I_{\rm rf}}{2\alpha\omega^{+}} R_{\rm AMR} \tau_{\rm DL}^{0} \sin 2\phi_{0} \cos \phi_{0},$$

$$V_{A} = \frac{I_{\rm rf}}{2\alpha\omega^{+}} R_{\rm AMR} \frac{\omega_{2}}{\omega} \tau_{z}^{0} \sin 2\phi_{0} \cos \phi_{0}.$$
(7)

 $I_{\rm rf}$  is the total microwave current that flows through the bilayer,  $\omega^+ = \gamma (2B_0 + \mu_0 M_{\rm eff})$ ,  $R_{\rm AMR}$  is the amplitude of the anisotropic magnetoresistance of the whole bilayer, and  $\omega_2 = \gamma (B_0 + \mu_0 M_{\rm eff})$ . C is a constant voltage offset that is included to account for nonresonant signals. For samples with thick magnetic layers, there can also be a significant additional contribution to the symmetric resonance component from spin pumping or resonant heating and the inverse spin Hall effect [20], which we mention below.

The experimental signal-to-noise ratio is significantly increased by modulating of the microwave amplitude; this is captured by letting  $V_{\rm mix}(I_{\rm rf}) \to V_{\rm mix}[I_{\rm rf}(1+\mu\cos\omega_m t)] \approx V_{\rm mix} + 2\mu V_{\rm mix}\cos\omega_m t$ , where  $\mu \in [0,1]$  is the AM depth. A lock-in amplifier demodulates the total signal by mixing with a  $\cos\omega_m t$  reference and applying a low-pass filter. The AM signal is therefore simply  $2\mu V_{\rm mix}$ .

If, alternatively, frequency modulation is used instead of amplitude modulation, the expected FM signal can be derived in a similar manner. We let  $V_{\rm mix}(\omega) \to V_{\rm mix}(\omega + \delta\omega\cos\omega_m t)$ , where  $\delta\omega\ll\omega$ ; this admits the simple expansion near the microwave carrier frequency,  $\omega_c$ ,

$$V_{\text{mix}}^{\text{FM}}(\omega) = V_{\text{mix}}(\omega + \delta\omega\cos\omega_m t) \Longrightarrow$$

$$V_{\text{mix}}^{\text{FM}}(\omega) \approx V_{\text{mix}}(\omega_c) + \frac{dV_{\text{mix}}}{d\omega}\big|_{\omega=\omega_c} \delta\omega\cos\omega_m t. \tag{8}$$

 $V_{\rm mix}^{\rm FM}$  is again demodulated by a lock-in amplifier, which leaves us with only  $(dV_{\rm mix}/d\omega)|_{\omega=\omega_c}\delta\omega$ . Therefore, the ratio of the detected mixing signal to the amplitude of the

frequency modulation is given by

$$\begin{split} V_{\text{mix}}^{\text{FM}}/\delta\omega &= \frac{\partial V_{\text{mix}}}{\partial\omega}\big|_{\omega=\omega_c} \\ &= \frac{\partial V_S}{\partial\omega}S + \frac{\partial V_A}{\partial\omega}A + \frac{1}{\omega_c}\left[2V_SA^2 + V_A\left(2A^3/S - A\right)\right] \\ &+ \frac{\omega_c}{M_{\text{eff}}\gamma^2\Delta}\left[2V_SSA + V_A\left(A^2 - S^2\right)\right] + C. \end{split} \tag{9}$$

Here we used  $\partial_{\omega}S = 2S\left[(1-S)\partial_{\omega}\Delta + A\partial_{\omega}B_0\right]/\Delta$  and  $\partial_{\omega}A = \left[A(1-2S)\partial_{\omega}\Delta - (S+2A^2)\partial_{\omega}B_0\right]/\Delta$ . Equation (9) is nearly identical to a previously derived result where the magnetic field was modulated [12]. Compared with the AM result, Eq. (6), the FM result has two additional fit parameters,  $dV_S/d\omega$  and  $dV_A/d\omega$ , to account for the possible frequency dependence of microwave transmission through the measuring circuit to the device.

### A. LS analysis

After measurement with either amplitude modulation or frequency modulation and then fitting of the ST FMR to determine  $V_S$  and  $V_A$  with use of either Eq. (6) or Eq. (9), the torque efficiencies may be determined directly from Eq. (7) if  $I_{\rm rf}$  is well calibrated, since the other parameters in Eq. (7) are independently measurable. However, since it is often challenging to determine accurately the value of  $I_{\rm rf}$  within the sample, we generally prefer to determine the torque efficiencies by taking appropriate ratios of  $V_S$  and  $V_A$  [8]. We first calculate an intermediate quantity,  $\xi_{\rm FMR}$ , defined as

$$\xi_{\rm FMR} = \frac{V_S}{V_A} \frac{e\mu_0 M_s t_N t_F}{\hbar} \sqrt{1 + \frac{\mu_0 M_{\rm eff}}{B_0}}.$$
 (10)

By use of Eqs. (2), (3), and (10), as long as the torque efficiencies are independent of the ferromagnetic layer thickness in the range of thickness we analyze, then  $\xi_{FMR}$  can be related to the dampinglike and fieldlike torque efficiencies as [8]

$$\frac{1}{\xi_{\text{FMR}}} = \frac{1}{\xi_{\text{DL}}} \left( 1 + \frac{\hbar}{e} \frac{\xi_{\text{FL}}}{\mu_0 M_s t_N t_F} \right). \tag{11}$$

Therefore, by taking results from a series of samples with different ferromagnet thicknesses,  $t_F$ , we can determine  $\xi_{\rm DL}$  and  $\xi_{\rm FL}$  from a linear fit of  $1/\xi_{\rm FMR}$  versus  $1/t_F$ .

# B. LW analysis: change of linewidth versus direct current

In dc-biased ST FMR, a direct current is applied parallel to the microwave current such that the dampinglike torque from the direct current rescales the effective Gilbert damping of the magnetic layer and causes the resonance linewidth to change linearly as a function of  $I_{dc}$ . The dampinglike SOT efficiency can be calculated from dc linewidth modulation as [5,11]

$$\xi_{\rm DL} = \frac{eM_s \omega^+ t_F}{\hbar \omega_c \sin \phi_0} \frac{W t_N}{x} \frac{d\Delta}{dI_{\rm dc}},\tag{12}$$

where W is the width of the current-carrying channel and x is the fraction of the total direct current that flows through the heavy metal.

#### III. MEASUREMENTS

All our samples are grown by dc-magnetron sputtering (in a system with base pressure less than  $4 \times 10^{-8}$  Torr) onto a surface-passivated high-resistivity Si wafer ( $\rho > 20\,000~\Omega$  cm). Each sample is grown in an independent deposition. The samples described in the main text have the stacking order:substrate/Ta(1 nm)/Pt(6 nm)/Py( $t_F$ )/Al(1 nm), with the magnetic layer being permalloy (Ni<sub>81</sub>Fe<sub>19</sub>). Ta is used as a seed layer to promote smooth growth and Al, which is oxidized on exposure to air, is used as a capping layer to prevent oxidation of Py. Pt ( $\rho = 20.4~\mu\Omega$  cm) and Py ( $\rho = 25~\mu\Omega$  cm) are far more conductive than Ta or oxidized Al, so we assume all of the current flows through just the Pt and Py layers. Analogous results for which Py is replaced by Co<sub>40</sub>Fe<sub>40</sub>B<sub>20</sub> can be found in Supplemental Material [21].

After growth, we pattern the samples into rectangular bars of different dimensions using photolithography and Ar-ion milling. The devices have dimensions  $40 \times 80~\mu\text{m}^2$ ,  $20 \times 60~\mu\text{m}^2$ , or  $20 \times 80~\mu\text{m}^2$ . All measurements shown in this work are taken on  $20 \times 80~\mu\text{m}^2$  devices, and the quantitative conclusions do not depend on the device geometry. We attach Ti(3 nm)/Pt(75 nm) contacts to the devices by another step of photolithography, dc-magnetron sputtering, and lift-off.

All data shown are measured on microwave-compatible Hall-bar structures that allow measurements of both longitudinal and transverse mixing voltages, as described in Ref. [20]. Here we analyze only the longitudinal mixing voltages, as that is the usual ST-FMR measurement geometry. The devices are connected to the circuit shown in Fig. 1(b). An rf source inputs a microwave current into the device through the ac port of a bias tee with either amplitude modulation or frequency modulation [Fig. 1(a)], while the magnitude of an external magnetic field is swept at a fixed angle  $\phi_0$  through the Kittel resonance condition. The dc voltage along the longitudinal direction generated by mixing is detected with a lock-in amplifier that references the modulating signal. For the dc-biased measurements, an additional direct current is applied through the dc port of the bias tee to flow through the device in addition to the microwave current. All measurements are performed at room temperature.

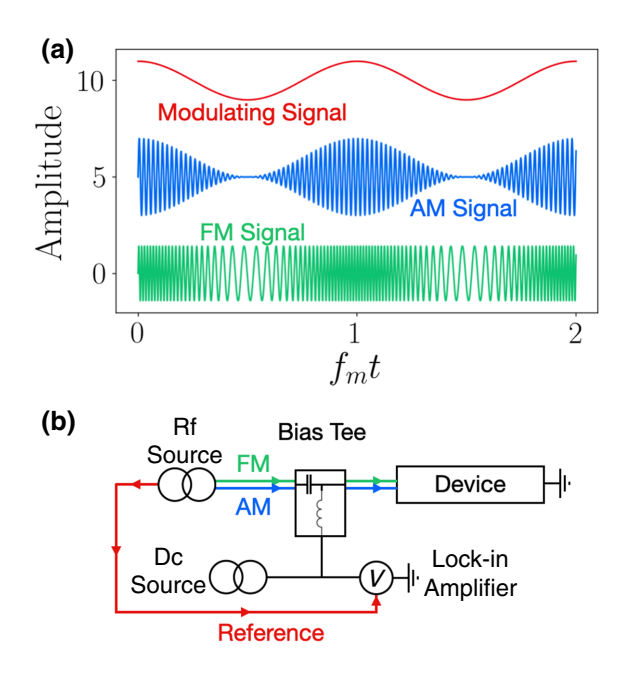


FIG. 1. The measurement setup used in this work. (a) Schematic representations of the time dependence of microwave current that is injected into the device under test for amplitude-modulated and frequency-modulated experiments. Offsets are added and the scale of the frequency modulation is exaggerated for clarity. (b) The circuit used in this measurement. The colors of the wires correspond to the colors of the signals in the top panel that the wire carries.

Measurements reported in the main text are performed at a carrier frequency of 10 GHz ( $f_c = \omega_c/2\pi$ ). The modulating signal for both AM and FM measurements is applied at a modulation frequency of 1.7 kHz ( $f_m = \omega_m/2\pi$ ). The external magnetic field is applied at  $\phi_0 = 45^{\circ}$  with respect

to the direction of applied microwave current. The AM measurements are done with 100% AM depth as depicted in Fig. 1(a) to maximize the measured signal. We find that reducing the AM depth has no effect on the results shown (see Fig. 13 in Supplemental Material [21]). The FM measurements are done with a frequency deviation ( $\delta f = \delta \omega/2\pi$ ) of 16 MHz. AM and FM are both applied by the internal circuitry of the rf source (Agilent 8257D). The 16-MHz frequency deviation and the modulation frequency of 1.7 kHz are both far smaller than the carrier frequency of 10 GHz, so in either measurement mode the modulation has a negligible effect on the microwave current over one precession cycle, a key assumption of the modeling.

## A. Results of lineshape analyses

Examples of the longitudinal resonant mixing signals from a Pt(6 nm)/Py(5 nm) sample for both AM and FM measurements are shown in Fig. 2. The AM measurement [Fig. 2(a)] is fit to Eq. (6) with the five fit parameters  $V_S$ ,  $V_A$ , C,  $B_0$ , and  $\Delta$ , while the FM measurement [Fig. 2(b)] is fit to Eq. (9) with the two additional fit parameters  $dV_S/d\omega$  and  $dV_A/d\omega$ . The fit to the AM measurement looks good by eye, but the best fit nevertheless produces significant systematic residuals ( $V_{\rm mix}^{\rm measured} - V_{\rm mix}^{\rm best fit}$ ), which hints that the framework of conventional ST-FMR analysis [Eq. (6)] gives an incomplete description.

To rule out spurious measurement artifacts, we repeat the AM measurements on three independent ST-FMR apparatuses at Cornell University and also perform measurements on different sample stacks; all of these measurements show the same systematic residuals for the AM fits. In contrast, for the FM measurements, the scale of the residuals after fitting to Eq. (9) is significantly smaller

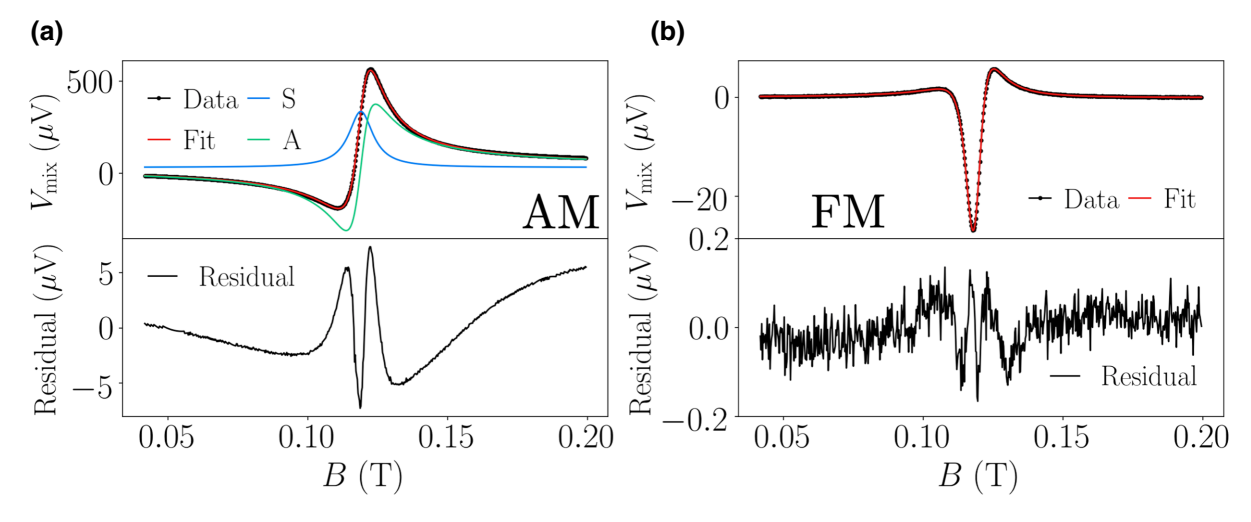


FIG. 2. Examples of measured resonances and fit residuals for a Pt(6 nm)/Py(5 nm) sample at 20 dBm, 10 GHz,  $\phi_0 = 45^\circ$ ,  $f_m = 1.7$  kHz, and  $I_{dc} = 0$ . (a) AM resonance taken at 100% AM depth with a fit to Eq. (6). (b) FM resonance taken at  $\Delta f = 16$  MHz with a fit to Eq. (9). The range of the magnetic field shown here corresponds to  $[B_0 - 15\Delta, B_0 + 15\Delta]$  for the primary resonance.

relative to the full signal magnitude. A more-complete discussion of the fit quality, residuals, and statistical details can be found in Supplemental Material [21].

For the AM fits in Fig. 2(a), we see that the residuals have a lineshape near the resonance field that closely resembles a Lorentzian derivative, suggesting that an additional parameter in Eq. (6) is varying at the modulation frequency and contributing to the homodyne mixing signal. Quantitative estimates suggest that a varying  $M_{\rm eff}$  will contribute far more than other candidate sample parameters and that  $M_{\rm eff}$  oscillating at the AM frequency, presumably due to heating, can result in the residual lineshape we observe near the resonance field. That is, suppose (in addition to the amplitude modulation of  $I_{\rm rf}$ ) that  $M_{\rm eff}$  also varies periodically as  $M_{\rm eff} \rightarrow M_{\rm eff} + \delta M_{\rm eff} \cos \omega_m t$ ; this, analogously to the frequency modulation, would allow the expansion

$$V_{\text{mix}}(M_{\text{eff}} + \delta M_{\text{eff}} \cos \omega_m t)$$

$$\approx V_{\text{mix}}(M_{\text{eff}}) + \frac{\partial V_{\text{mix}}}{\partial M_{\text{eff}}} \delta M_{\text{eff}} \cos \omega_m t. \tag{13}$$

The total mixing signal will thus consist of the sum of two terms that vary periodically with the AM,

$$\left(2\mu V_{\text{mix}} + \frac{\partial V_{\text{mix}}}{\partial M_{\text{eff}}} \delta M_{\text{eff}}\right) \cos \omega_m t, \tag{14}$$

and *both* will be demodulated by the lock-in amplifier. To confirm that the residuals can arise from heat-driven  $M_{\rm eff}$  oscillation, we measure  $M_{\rm eff}$  while heating the sample. We find that the measured  $M_{\rm eff}$  is sensitive to the sample temperature (see Fig. 11 in Supplemental Material [21]).

A homodyne signal from an oscillating value of  $M_{\rm eff}$ cannot by itself explain the full residuals in the AM fits; in addition the AM residuals appear to contain an ordinary AM resonance lineshape [Eq. (6)] with a very large linewidth. In Fig. 3 we show the fit residuals of an AM measurement taken on a Py(3 nm) sample (with no dc bias). We fit the residuals to the sum of a homodyne signal corresponding to an oscillating value of  $M_{\text{eff}}$  (green curve) and a large- $\Delta$  resonant background [Eq. (6)] (blue curve) with  $\Delta_{\text{large}} = 41.6 \text{ mT}$ , much larger than the  $\Delta = 7.3 \text{ mT}$ for the primary resonance. The sum of the two contributions (red curve) fits the residuals very well. On the basis of direct measurements of  $M_{\text{eff}}$  versus temperature on the same device  $[d(\mu_0 M_{\text{eff}})/dT = 8 \times 10^{-4} \text{ T/°C}]$ , the scale of the temperature oscillations needed to produce the oscillating- $M_{\rm eff}$  homodyne signal is approximately 1 °C (see Supplemental Material [21]).  $V_S$  and  $V_A$  for the large- $\Delta$  resonance for the data in Fig. 2 are 12 and 7  $\mu$ V, respectively, while for the primary resonance  $V_S = 311 \mu V$  and  $V_A = 684 \,\mu V$ .

We consider two options for the origin of the large- $\Delta$  resonance: a region of increased damping near the sample

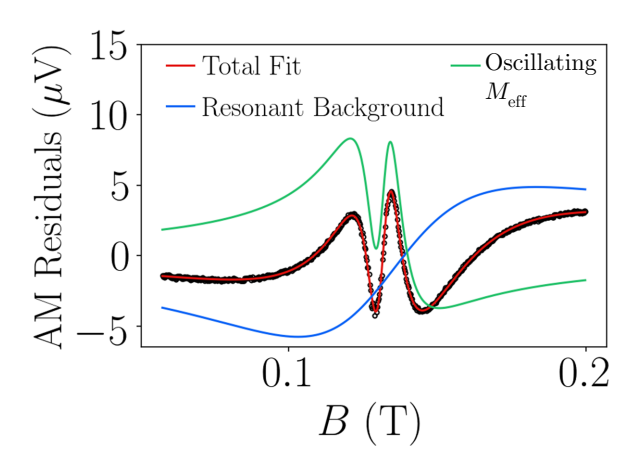


FIG. 3. (a) Measured fit residuals for an AM measurement of a Py(3 nm) sample taken at zero dc bias, with a fit to the sum of contributions from a heating-induced oscillation of  $M_{\rm eff}$  and a large- $\Delta$  resonant background. The linewidth of the primary resonance for Py(3 nm) samples is greater than for Py(5 nm) samples, so the range of the magnetic field shown here still corresponds to  $[B_0 - 15\Delta, B_0 + 15\Delta]$  for the primary resonance.

edges or a region of increased damping near a magnetic interface. If the origin were due to increased damping near the sample edges, we would expect the ratio of the amplitudes for the large- $\Delta$  and primary resonances to scale inversely with the sample width and to be approximately independent of the ferromagnetic layer thickness. Instead, we find that this ratio is insensitive to the sample width (a change of less than 10% in the symmetric component and less than 4% in the antisymmetric component when the sample width is changed by a factor of 2), while it is sensitive to the ferromagnetic layer thickness (see Fig. 12 in Supplemental Material [21]). This suggests that the portion of the sample with increased damping is an interfacial region. Additional evidence for an origin associated with the heavy-metal-ferromagnet interface comes from the fact that the large- $\Delta$  linewidth is very sensitive to the applied direct current (see Fig. 12 in Supplemental Material [21]), which is consistent with a very thin and/or low-moment region under the influence of the spin current generated by the heavy metal.

Our observations might be related to recent findings from an IBM group regarding interfacial regions in  $Co_{40}Fe_{40}B_{20}/MgO/Co_{40}Fe_{40}B_{20}$  magnetic tunnel junctions whose dynamics can become partially decoupled from the dynamics of the bulk of the magnetic films [22,23]. The two experiments differ, however, in that the IBM work deduced a difference in effective magnetic anisotropy (compared with the bulk of the magnetic film) for the interfacial layers at  $Co_{40}Fe_{40}B_{20}/MgO$  interfaces, while in our devices the large- $\Delta$  resonance corresponds to increased damping near a Pt/ferromagnet interface without a large difference in anisotropy.

We suggest that there are two reasons why the fit residuals for the FM measurements are reduced compared with the AM measurements. First, temperature oscillations at the modulation frequency will be smaller for the FM measurements because the magnitude of  $I_{\rm rf}$  will be approximately constant in time, so Ohmic heating caused by  $I_{\rm rf}$ will also be approximately constant rather than oscillating at the modulation frequency. Temperature oscillations will not be eliminated completely however, since FM near the resonance will cause the energy absorbed by resonant heating of the magnetic layer (energy transfer associated with magnetic excitation by the current-induced torques) to oscillate at the modulation frequency. We suggest that this resonant heating is likely the main cause of the small remaining systematic residuals near the resonance field in the fits to the FM data [Fig. 2(b)]. Second, contributions from the large- $\Delta$  resonance to the FM measurements are reduced precisely because the linewidth is so broad, so this part of the signal is relatively insensitive to variations in the applied frequency.

If one proceeds with the standard ST-FMR macrospin analysis—Eqs. (10) and (11)—(ignoring the residuals for now), the resulting values of  $1/\xi_{\rm FMR}$  for the AM measurements and the FM measurements are shown in Fig. 4 for samples with ferromagnetic layer thicknesses  $t_F$  ranging from 2 to 10 nm. The samples with the thickest ferromagnetic layers ( $t_F \geq 8$  nm) show deviations from a linear dependence of  $1/\xi_{\rm FMR}$  versus  $1/t_F$  that can be understood as due to the effect of an inverse spin Hall voltage resulting from spin pumping or resonant heating [8,20]. We therefore perform the linear fits only for the four samples with the thinnest ferromagnetic layers, extracting the

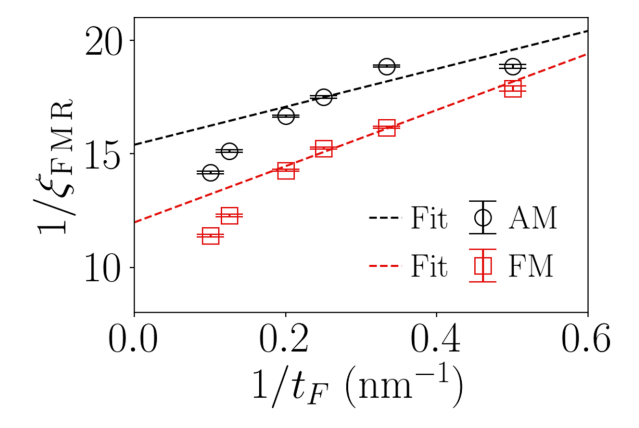


FIG. 4. Fits to Eq. (11) to determine the spin-torque efficiencies  $\xi_{\rm DL}$  and  $\xi_{\rm FL}$  from the lineshape analyses. The values of  $\xi_{\rm FMR}$  plotted are calculated according to Eq. (10), corresponding to measurements of  $V_S$  and  $V_A$  done at 20 dBm, 10 GHz,  $\phi_0=45^\circ$ ,  $f_m=1.7\,$  kHz, and  $I_{\rm dc}=0$ . The resonance fits are performed over the same window as the LW measurements:  $[B_0-15\Delta,B_0+15\Delta]$ . AM measurements are done with 100% AM depth and FM measurements are done with  $\delta f=16\,$  MHz.

TABLE I.  $\xi_{DL}$  and  $\xi_{FL}$  that result from the linear fits shown in Fig. 4.

	AM	FM
ξ <sub>DL</sub>	0.0650(4)	0.0835(7)
ξ <sub>FL</sub>	0.0050(2)	0.0094(2)

values shown in Table I.  $\xi_{DL}$  and  $\xi_{FL}$  are calculated from the y intercept and slope of the fits, respectively, following the prescription of Eq. (11). The FM and AM methods yield values for both  $\xi_{DL}$  and  $\xi_{FL}$  that differ by considerably more than the estimated statistical uncertainty in the results. The difference in the values of  $\xi_{DL}$  is about 30%, while for  $\xi_{FL}$  the FM result is nearly double the AM result.

We suggest that the differences between these AM and FM LS results can be explained by the ignoring of the residual terms. If we take the values of  $\xi_{DL}$  and  $\xi_{FL}$  determined by the FM measurements and use them in the fitting to the AM data, the result is a residual similar to that shown in Fig. 3 that can be fit just as well to a sum of a signal due to an oscillating value of  $M_{\rm eff}$  and a large- $\Delta$  resonance (see Fig. 5 in Supplemental Material [21]). Fits to the AM data that include both the primary resonance and the two artifact contributions therefore possess near-degenerate fitting parameters, which can make determination of the spin-torque efficiencies imprecise.

# B. Results of linewidth analyses

The LW measurement proceeds identically to the LS measurement, except for the application of a direct current parallel to the microwave current. A full resonance lineshape (e.g., Fig. 2) is collected for direct currents ranging from -4 to 4 mA and the resonances are fit to Eq. (6) for the AM measurements or Eq. (9) for the FM measurements to extract the linewidth,  $\Delta$  (ignoring residuals for now). We find that the value of  $\Delta$  that we get from the fits for the AM measurement depends strongly on whether and to what extent we include the tails of the resonance. Figure 5 shows the current dependence of linewidths for a Pt(6 nm)/Py(5 nm) sample extracted from fits over the field range  $[B_0 - 15\Delta, B_0 + 15\Delta]$  (with  $\Delta$  adjusted for each sample corresponding to the linewidth of the primary resonance at zero direct current). This is the largest fit window that is possible while consistently excluding artifacts associated with deviations from magnetic saturation at low field for all samples. The zero-current value of  $\Delta$ is subtracted from each of the plots in Fig. 5 to highlight the difference in the slopes of the best-fit lines. We apply Eq. (12) to the slopes of the best-fit lines and get the results for  $\xi_{DL}$  shown in Table II.

For this sample, we see that the FM LW measurements agree with the FM LS results within the experimental uncertainties (Table II), while the AM LW measurements differ by more than a factor of 3 from both the FM

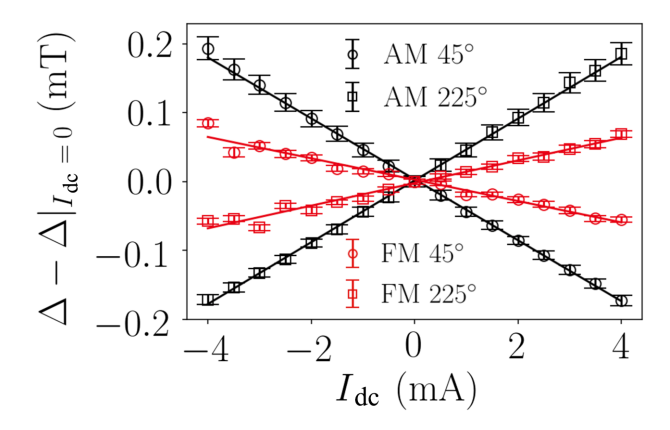


FIG. 5. Dependence of the resonance linewidth ( $\Delta$ ) on  $I_{\rm dc}$  for a Pt(6 nm)/Py(5 nm) sample based on fits to Eq. (6) for the AM measurements and Eq. (9) for the FM measurements for data collected at 20 dBm, 10 GHz,  $\phi_0 = 45^{\circ}/225^{\circ}$ , and  $f_m = 1.7$  kHz. Linewidths are extracted using the fit window [ $B_0 - 15\Delta$ ,  $B_0 + 15\Delta$ ]. The zero-dc linewidths (5.27 mT for AM and 5.24 mT for FM) are subtracted. The solid lines are least-squares best-fit lines to the data.

results and the AM LS measurements. Figure 6 compares the results of similar LW analyses for all of the Pt(6 nm)/Py( $t_F$ ) samples with different magnetic layer thicknesses using the same fit window [ $B_0 - 15\Delta$ ,  $B_0 + 15\Delta$ ]. The AM LW measurements (black points) give far-larger values for  $\xi_{DL}$  compared with any of the other techniques. The FM LW measurements are reasonably consistent with the FM LS value in the  $t_F$  range from 4 to 10 nm (with small deviations for  $t_F = 10$  nm possibly due to the ignoring of an inverse spin Hall voltage generated by spin pumping or a spin Seebeck effect), but the FM LW measurements also differ increasingly from the LS results for Py thicknesses below 4 nm.

In Fig. 7 we show the results of the same LW analysis using different sizes for the window of the magnetic field included in the fits. The panels on the left show the values of  $\xi_{DL}$  extracted for window sizes from  $[B_0 - 15\Delta, B_0 + 15\Delta]$  to  $[B_0 - 2\Delta, B_0 + 2\Delta]$ . For the AM and FM data sets, the extracted values of  $\xi_{DL}$  decrease with decreasing window size. We interpret this dependence as a clear indication that the LW analysis can be disrupted by the long tails of the residual terms that are not included as part of the standard linewidth analysis. For a fixed value of fit-window size, the disruption is severest for magnetic

TABLE II.  $\xi_{DL}$  values for a Pt(6 nm)/Py(5 nm) sample obtained with the LW method. The values are extracted from the slopes of the best-fit lines in Fig. 5 and Eq. (12).

ξ <sub>DL</sub>	AM	FM
45°	0.234(5)	0.082(2)
225°	0.237(5)	0.087(2)

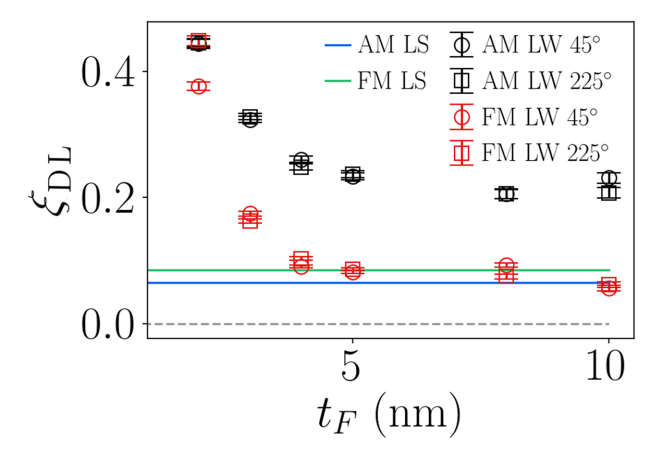


FIG. 6. Extracted values of the dampinglike spin-torque efficiency  $\xi_{\rm DL}$  for samples with different ferromagnetic layer thicknesses. Symbols show the results of the AM and FM linewidth analyses using fits over the field range  $[B_0-15\Delta,\,B_0+15\Delta]$ . The green and blue lines are the results of the lineshape analyses for the thickness series shown in Fig. 4.

layers thinner than 4 nm because the linewidth of the primary resonance increases for thin layers, making the primary resonance more difficult to disentangle from the large-linewidth residual signal.

The right panels in Fig. 7 show enlargements of the same LW results to better visualize the extrapolation of the measurements to zero linewidth. We find that this extrapolation brings the results of the AM LW and FM LW analyses

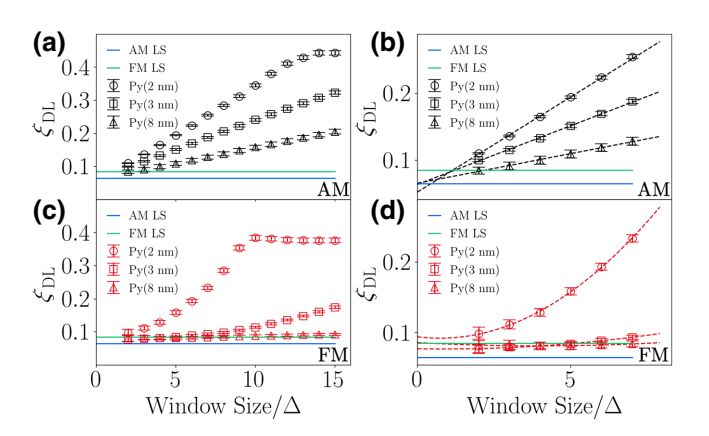


FIG. 7. The dampinglike SOT efficiency,  $\xi_{DL}$ , versus the size of the fit window (normalized by the resonance linewidth,  $\Delta$ ). All data in this figure are from the LW-analysis method with  $\phi_0 = 45^{\circ}$ . (a) The full range of fit windows with AM. (b) An enlarged view of the AM data with best-fit lines superimposed.  $\xi_{DL}$  is linear in the fit window, and the y intercept of the best-fit lines agrees well with the corresponding result of the AM LS analysis. (c) The full range of fit windows with FM. (d) An enlarged view of the FM data with best-fit second-degree polynomials superimposed.  $\xi_{DL}$  is quadratic in the fit window, and the y intercept of the best-fit lines agrees well with the corresponding result of the FM LS analysis.

into reasonable quantitative agreement with the lineshape results.

We emphasize that the sensitive dependence on fitwindow size shown by Fig. 7 occurs even though the individual fits look quite good by eye for any choice of window size. The LW analyses are based on quite subtle changes in the resonance lineshape (e.g., about a 2% change in linewidth over the full range of  $I_{dc}$  for the FM measurements shown in Fig. 5). Therefore, even small changes in  $V_{\text{mix}}$  associated with current-dependent residuals can affect the LW analysis—the small tails of the ST FMRs can be substantially affected even if the overall magnitude of the residual signals near the resonance field is small. The large- $\Delta$  resonance in particular has a large effect on the LW analyses because its linewidth is strongly current dependent (see Fig. 12 in Supplemental Material [21]). This is why the windowed fitting works—as the window size is reduced the strong current dependence associated with the tails of the large- $\Delta$  residual signal is excluded.

We try fitting the AM resonances to a generalized form of Eq. (6) that includes the models for the residuals directly in the fit, but this is not able to provide improved quantitative results because of near-degenerate fit parameters. We therefore recommend the procedure depicted in Fig. 7 as the simplest approach to improving ST-FMR linewidth analyses—performing the standard ST FMR fits using a series of different fit-window sizes, followed by extrapolation to small windows to minimize the influence of the large-linewidth residuals.

# IV. CONCLUSIONS

We identify a cause of inconsistencies between measurements of spin-orbit torque determined via lineshape and linewidth analyses of ST-FMR data—that the standard model for analyzing ST-FMR data does not fully account for all of the magnetic dynamics that can affect the measurements. The standard analysis leaves residuals that we identify as due to (i) current-induced excitation of a magnetic mode with larger damping than the bulk of the magnetic layer and also (ii) temperature oscillations (approximately 1 °C) associated with the modulation schemes used for lock-in amplifier measurements. The residuals are not large, with amplitudes on the of order 1% of the primary resonance, but nevertheless they can affect the current dependence of the resonance tails sufficiently to disrupt an extraction of the antidamping spinorbit torque efficiency based on the current dependence of the ST-FMR linewidth. The influence of the largelinewidth residuals can be minimized by performing the standard lineshape analysis using different choices for the range of magnetic field values used to fit the ST FMRs, followed by extrapolation to zero fit window. We recommend this procedure for all future uses of LW analysis. The effect of the residuals can also be reduced by performing ST-FMR measurements using frequency modulation rather than amplitude modulation, but frequency modulation alone does not cure inconsistencies between the lineshape and linewidth results for our thinnest magnetic layers without extrapolation of the fit window to small values.

The microscopic origin of the large-linewidth mode that contributes to the residual signal remains an interesting open question. On the basis of the scaling of signal amplitudes with the widths and thicknesses of our samples, we identify this mode as being due to the heavy-metal-magnet interface rather than as being due to increased damping at the lateral edges of our magnetic layers. It is therefore possible that this mode is due to an interface magnon or magnetic impurities caused by intermixing near the interface. We also consider whether it might be due to a magnetic proximity layer within the platinum, but amplitude-modulated ST-FMR measurements on a W(3 nm)/Py(5 nm) sample also exhibit a contribution from a large-linewidth resonance (see Fig. 7 in Supplemental Material [21]). Since magnetic proximity effects should be negligible in W at room temperature, this argues against this mechanism as the dominant contribution in the Pt samples. Future experiments with variation of the interface structure or with the insertion of spacer layers might help to reveal the origin of the large-linewidth mode.

# **ACKNOWLEDGMENTS**

This research was funded by the U.S. Department of Energy (DE-SC0017671). The work was performed in part at the Cornell NanoScale Facility, a member of the National Nanotechnology Coordinated Infrastructure, which is supported by the National Science Foundation (Grant No. NNCI-2025233), and in part at the Cornell Center for Materials Research Shared Facilities, which are supported through the National Science Foundation MRSEC program (Grant No. DMR-1719875).

- [1] I. M. Miron, K. Garello, G. Gaudin, P.-J. Zermatten, M. V. Costache, S. Auffret, S. Bandiera, B. Rodmacq, A. Schuhl, and P. Gambardella, Perpendicular switching of a single ferromagnetic layer induced by in-plane current injection, Nature 476, 189 (2011).
- [2] L. Liu, C. F. Pai, Y. Li, H. W. Tseng, D. C. Ralph, and R. A. Buhrman, Spin-torque switching with the giant spin Hall effect of tantalum, Science 336, 555 (2012).
- [3] K. L. Wang, J. G. Alzate, and P. K. Amiri, Low-power non-volatile spintronic memory: STT-RAM and beyond, J. Phys. D: Appl. Phys. 46, 074003 (2013).
- [4] F. Oboril, R. Bishnoi, M. Ebrahimi, and M. B. Tahoori, Evaluation of hybrid memory technologies using sot-mram for on-chip cache hierarchy, IEEE Trans. Comput.-Aided Des. Integr. Circ. Syst. 34, 367 (2015).

- [5] L. Liu, T. Moriyama, D. C. Ralph, and R. A. Buhrman, Spin-Torque Ferromagnetic Resonance Induced by the Spin Hall Effect, Phys. Rev. Lett. 106, 036601 (2011).
- [6] A. R. Mellnik, J. S. Lee, A. Richardella, J. L. Grab, P. J. Mintun, M. H. Fischer, A. Vaezi, A. Manchon, E.-A. Kim, N. Samarth, and D. C. Ralph, Spin-transfer torque generated by a topological insulator, Nature 511, 449 (2014).
- [7] M. Harder, Z. X. Cao, Y. S. Gui, X. L. Fan, and C.-M. Hu, Analysis of the line shape of electrically detected ferromagnetic resonance, Phys. Rev. B 84, 054423 (2011).
- [8] C. F. Pai, Y. Ou, L. H. Vilela-Leão, D. C. Ralph, and R. A. Buhrman, Dependence of the efficiency of spin Hall torque on the transparency of Pt/ferromagnetic layer interfaces, Phys. Rev. B 92, 064426 (2015).
- [9] K. Ando, S. Takahashi, K. Harii, K. Sasage, J. Ieda, S. Maekawa, and E. Saitoh, Electric Manipulation of Spin Relaxation Using the Spin Hall Effect, Phys. Rev. Lett. 101, 036601 (2008).
- [10] S. Kasai, K. Kondou, H. Sukegawa, S. Mitani, K. Tsukagoshi, and Y. Otani, Modulation of effective damping constant using spin Hall effect, Appl. Phys. Lett. 104, 092408 (2014).
- [11] T. Nan, S. Emori, C. T. Boone, X. Wang, T. M. Oxholm, J. G. Jones, B. M. Howe, G. J. Brown, and N. X. Sun, Comparison of spin-orbit torques and spin pumping across NiFe/Pt and NiFe/Cu/Pt interfaces, Phys. Rev. B 91, 214416 (2015).
- [12] A. M. Gonçalves, I. Barsukov, Y.-J. Chen, L. Yang, J. A. Katine, and I. N. Krivorotov, Spin torque ferromagnetic resonance with magnetic field modulation, Appl. Phys. Lett. **103**, 172406 (2013).
- [13] W. Skowroński, T. Nozaki, Y. Shiota, S. Tamaru, K. Yakushiji, H. I. Kubota, A. Fukushima, S. Yuasa, and Y. Suzuki, Perpendicular magnetic anisotropy of Ir/CoFeB/MgO trilayer system tuned by electric fields, Appl. Phys. Express 8, 053003 (2015).

- [14] C. J. Safranski, Y.-J. Chen, I. N. Krivorotov, and J. Z. Sun, Material parameters of perpendicularly magnetized tunnel junctions from spin torque ferromagnetic resonance techniques, Appl. Phys. Lett. 109, 132408 (2016).
- [15] C. Safranski, E. A. Montoya, and I. N. Krivorotov, Spin-orbit torque driven by a planar Hall current, Nat. Nanotechnol. 14, 27 (2018).
- [16] Y.-J. Chen, H. K. Lee, R. Verba, J. A. Katine, I. Barsukov, V. Tiberkevich, J. Q. Xiao, A. N. Slavin, and I. N. Krivorotov, Parametric resonance of magnetization excited by electric field, Nano. Lett. 17, 572 (2016).
- [17] J. W. Xu and A. D. Kent, Charge-To-Spin Conversion Efficiency in Ferromagnetic Nanowires by Spin Torque Ferromagnetic Resonance: Reconciling Lineshape and Linewidth Analysis Methods, Phys. Rev. Appl. 14, 014012 (2020).
- [18] D. MacNeill, G. M. Stiehl, M. H. D. Guimarães, N. D. Reynolds, R. A. Buhrman, and D. C. Ralph, Thickness dependence of spin-orbit torques generated by wte<sub>2</sub>, Phys. Rev. B 96, 054450 (2017).
- [19] C. Kittel, On the theory of ferromagnetic resonance absorption, Phys. Rev. 73, 155 (1948).
- [20] S. Karimeddiny, J. A. Mittelstaedt, R. A. Buhrman, and D. C. Ralph, Transverse and Longitudinal Spin-Torque Ferromagnetic Resonance for Improved Measurement of Spin-Orbit Torque, Phys. Rev. Appl. 14, 024024 (2020).
- [21] See Supplemental Material at <a href="http://link.aps.org/supplemental/10.1103/PhysRevApplied.15.064017">http://link.aps.org/supplemental/10.1103/PhysRevApplied.15.064017</a> for additional information concerning film properties, measurements on other film stacks, and details of the residual signals.
- [22] J. Z. Sun, Resistance-area product and size dependence of spin-torque switching efficiency in CoFeB-MgO based magnetic tunnel junctions, Phys. Rev. B 96, 064437 (2017).
- [23] C. Safranski and J. Z. Sun, Interface moment dynamics and its contribution to spin-transfer torque switching process in magnetic tunnel junctions, Phys. Rev. B **100**, 014435 (2019).